Excitonic and charge transfer interactions in tetracene stacked and T-shaped dimers

Daniel C. A. Valente, Mariana T Do Casal, Mario Barbatti, Thomas A Niehaus, Adelia J A Aquino, Hans Lischka, Thiago M Cardozo

Excitonic and Charge Transfer Interactions in Tetracene Stacked and T-shaped Dimers[1]

Daniel C. A. Valente[1], Mariana T. do Casal[2], Mario Barbatti[2], Thomas A. Niehaus[3], Adelia J. A. Aquino[4,5], Hans Lischka[5,6,a)], Thiago M. Cardozo[1,a)]

[1]Instituto de Química, Universidade Federal do Rio de Janeiro, Rio de Janeiro, Rio de Janeiro, Brazil.
[2]Aix Marseille University, CNRS, ICR, Marseille, France.
[3]Univ Lyon, Université Claude Bernard Lyon 1, CNRS, Institut Lumière Matière, F-69622, Villeurbanne, France.
[4]Department of Mechanical Engineering, Texas Tech University, Lubbock, Texas, USA.
[5]School of Pharmaceutical Sciences and Technology, Tianjin University, Tianjin, People's Republic of China.
[6]Department of Chemistry and Biochemistry, Texas Tech University, Lubbock, Texas, USA.
[a)]Authors to whom correspondence should be addressed: thiago@iq.ufrj.br; Hans.Lischka@ttu.edu

ABSTRACT

Extended quantum chemical calculations were performed for the tetracene dimer to provide benchmark results, analyze the excimer survival process, and explore the possibility of using long-range-corrected (LC) time-dependent (TD) second-order density functional tight-biding (DFTB2) for this system. Ground- and first-excited-states optimized geometries, vertical excitations at relevant minima, and intermonomer displacement potential energy curves (PECs) were calculated for these purposes. Ground-state geometries were optimized with the scaled-opposite-spin (SOS) second-order Møller-Plesset perturbation theory (MP2) and LC-DFT (density functional theory) and LC-DFTB2 levels. Excited-state geometries were optimized with SOS-ADC(2) (algebraic diagrammatic construction to second-order) and the time-dependent approaches for the latter two methods. Vertical excitations and PECs were

compared to multireference configuration interaction DFT (DFT/MRCI). All methods predict the lowest-energy S_0 conformer to have monomers parallel and rotated relative to each other and the lowest S_1 conformer to be of a displaced-stacked type. LC-DFTB2, however, presents some relevant differences regarding other conformers for S_0. Despite some state-order inversions, an overall good agreement between methods was observed in the spectral shape, state character, and PECs. Nevertheless, DFT/MRCI predicts that the S_1 state should acquire a doubly excited-state character relevant to the excimer survival process and, therefore, cannot be completely described by the single reference methods used in this work. PECs also revealed an interesting relation between dissociation energies and the intermonomer charge-transfer interactions for some states.

I. INTRODUCTION

Several potential advantages, such as low synthesis cost, have stimulated the search for organic optoelectronic materials.[1] Among these materials, a particularly important class is that of the polycyclic aromatic hydrocarbons (PAHs) due to their potential application as organic semiconductors[2] and their relevance for spintronics,[3] astrochemistry,[4] and nonlinear optics.[5] Tetracene and pentacene, in particular, are the focus of a renewed interest due to the singlet fission phenomenon[6] and the promise of increased efficiency in optoelectronic devices, with several reported theoretical[7–10] and experimental[11,12] studies focused on monomers and dimers of these molecules and their derivatives.

Multiple theoretical studies focused on tetracene monomers have been reported with various goals, including analyzing the biradical character of polyacenes[13,14] or their excited-state nonadiabatic dynamics.[15] The latter, for example, provided relevant information about the nonradiative relaxation mechanism after photoexcitation. Nevertheless, for singlet fission and other applications, the supramolecular properties of dimers and larger aggregates are also essential. Therefore, several studies

have tackled these systems in small aggregates and crystals,[7,16–22] in which excimer formation plays a central role. The latter process has been the subject of theoretical studies, such as for covalently linked tetracene dimers in the context of singlet fission,[23] but further investigation, especially delivering benchmark results, would prove beneficial for the unmodified tetracene dimer. Such benchmarks could be used to analyze the reliability of methods employed to simulate the excimer formation and survival and determine the most relevant intermonomer interactions.

For the generation of benchmark results, comparison with available experimental data is essential. Both geometric and spectroscopic properties of the tetracene dimer have been experimentally reported. Katul and Zahlan first showed that tetracene in solution could form dimers in the ground state, redshifting the lowest absorption band maximum from 2.6 to 2.3 eV.[24] A similar result has been reported by Iannone and Scott[25] (close to 2.6), who generated tetracene dimer by decomposing ditetracene in a solid host matrix. Fluorescence properties of tetracene change radically depending on its concentration in solution, going from a sharp peak localized at 2.6 eV at low concentrations to a structureless band that peaks around 2.2 eV.[24] Schouder et al.[26] have recently explored the ground-state structure of tetracene dimers using experimental and theoretical techniques. They concluded that two geometries are consistent with the angular dispersion data generated by Coulomb explosion experiments of tetracene dimers inside helium droplets. These two geometries corresponded to parallel monomers, but differing in the angle between their long axes (either 0 or 25º).

Besides experimental results, comparison with previous theoretical work is also essential, as numerous calculations on the tetracene dimer and similar systems (like pentacene dimer) or derivatives have been reported. A theoretical work on PAH sheets using explicitly correlated approaches predicted a tetracene dissociation energy (D_e) of -9.4 kcal/mol.[27] Zimmerman et al.[7] analyzed the excited state of tetracene and pentacene clusters, predicting a doubly excited state near the singly-excited S_1 state. Further work for tetracene and other molecules also predicted such a state to be present and relevant for singlet

fission.[8,10,23,28,29] Dynamics calculations have also been reported for tetracene dimers and higher oligomers,[20,30] providing relevant information on exciton (de)localization, as an example. Based on these and several other theoretical and experimental results, mechanisms for singlet fission have been proposed, as well as heuristic guidelines on how to properly search through theoretical calculations for new candidates exhibiting this process.[31]

In addition to the doubly excited state, other types of states have also been proposed as relevant for the singlet fission process, and a recent study by Suarez et al.[9] used descriptors[32–34] based on the first-order transition density matrix (1TDM) to study the importance of charge-transfer and charge-resonance states in this process for dimer conformations relevant for solid-state tetracene. This same technique can be applied to analyze the relevant interactions in the excimer survival process,[35–37] and, recently, Cardozo et al.[38] demonstrated through nonadiabatic excited-state dynamics the prominent role of intermolecular charge transfer in the excimer formation process for a benzene dimer.

Although several quantum chemical methods can be applied to calculating excited states for tetracene, the computational cost can quickly become prohibitive for aggregates. To reduce the costs, parameterized methods such as the second-order density functional-based tight-binding method (DFTB2[39]), in combination with its time-dependent (TD) formulation, may provide an alternative, particularly since the implementation of long-range corrections (LC-TD-DFTB2[40,41]). This approach has not yet been applied to model a tetracene dimer to the best of our knowledge. It has been successfully used to simulate the pyrene dimer photodynamics,[42] but it certainly needs more validation, which must be performed compared to calculations using higher-level methods.

The main objective of the present work is to benchmark theoretical results for the tetracene dimer. Different types of methods were included to explore this system: DFT/MRCI, SOS-ADC(2)/SOS-MP2, ADC(2), (TD-)ωB97X-D, (TD-)CAM-B3LYP, and the semiempirical LC-TD-DFTB2 and DFTB3 (see acronym definitions in the Computational Methods). Optimized geometries, vertical excitations, and

potential energy curves were calculated and compared. Available experimental results for dimer geometries and absorption and emission spectra were also included in this comparison. Lastly, results were also analyzed using electronic descriptors based on the 1TDM to characterize the states and determine the relevant interactions during the excimer survival.

II. COMPUTATIONAL METHODS

Ground-state geometry optimizations (S_0) for a tetracene dimer were performed with the scaled-opposite-spin version of the second-order Møller-Plesset (SOS-MP2[43]), with density functional theory (DFT) using the range- and dispersion-corrected functional ωB97X-D,[44] and with the long-range corrected second-order density functional-based tight-binding (LC-DFTB2). For each of these methods, optimization of the first excited state (S_1) and vertical excitations were computed with the corresponding excited-state approach: scaled-opposite-spin second-order algebraic diagrammatic construction (SOS-ADC(2)[45]) for SOS-MP2, linear-response time-dependent DFT (TD-ωB97X-D) for DFT, and LC-TD-DFTB2[41] for LC-DFTB2. Third-order DFTB (DFTB3[46]), TD-CAM-B3LYP,[47] and ADC(2)[48,49] were also applied. Combined density functional theory and multireference configuration interaction (DFT/MRCI[50,51]) calculations were used as the reference for vertical excitations due to previous encouraging results.[21,52,53] Vibrational frequencies were calculated with SOS-MP2/SOS-ADC(2), (TD-)ωB97X-D and, only for the ground state, with CAM-B3LYP. Symmetry was not imposed for dimer geometry optimizations but was used for vertical excitations since the predicted minima were symmetrical.

Approximated interaction energies were calculated as the difference between the dimer energy and the sum of the isolated monomers' electronic energies. S_1 excimer stabilization energies (ESE) were calculated as the difference between S_1 vertical excitation and S_1 adiabatic excitation energies. As usual, the former was calculated as the lowest excitation energy at the S_0-optimized geometry and the latter as

the electronic energy difference between S_0 and S_1 at their optimized geometries. Dissociation energies for each state (D_e) were estimated from potential energy curves as the difference in energy between the minimum energy structure and the structure with maximum intermonomer separation.

Charge transfer in a system can be quantified by the charge transfer value,[32,54] CT, defined in Equation 1:

$$\mathrm{CT} = \frac{1}{\Omega^I}\sum_{A,B\neq A}\Omega_{AB}^I \quad (1)$$

$$\Omega_{AB}^I = \frac{1}{2}\sum_{\mu\in A}\sum_{\nu\in B}\left[(D^{0I}S)_{\mu\nu}(SD^{0I})_{\mu\nu} + D_{\mu\nu}^{0I}(SD^{0I}S)_{\mu\nu}\right] \quad (2)$$

$$\Omega^I = \sum_{A,B}\Omega_{AB}^I \quad (3)$$

In Equations 1 to 3, A and B are fragments of the system, $\mathbf{D}^{0I}$ is the one-particle transition density matrix (1TDM) between the ground (0) and excited state (I), and **S** is the orbital overlap matrix. For each excited state, an omega matrix ($\mathbf{\Omega}^I$) can be defined by varying the indexes A and B through all the fragments of the system.

CT values, omega matrices, dominant orbital transitions, oscillator strengths, and symmetries were used to compare excited states between methods. However, the first two properties were not included for doubly excited states as these are not well represented by 1TDM only.

SOS-MP2, ADC(2), and SOS-ADC(2) were carried out with Turbomole[55,56] (versions 7.2 (mainly), 7.3, and 7.4) using the frozen core and the resolution of identity (RI)[57–59] approximations, and appropriate auxiliary basis sets.[60] (TD-)CAM-B3LYP and (TD-)ωB97X-D calculations were performed with ORCA[61,62] (version 4.2.1) and Gaussian 09,[63] respectively. RI with appropriate auxiliary basis sets,[64,65] increased grid (*grid4 finalgrid5*), and D3(BJ) dispersion corrections[66,67] were used with CAM-B3LYP functional.

In the DFT/MRCI calculations, as developed by Grimme and Waletzke[50] and redesigned by Marian et al.,[51,68–70] the R2018 hamiltonian[69] and a 0.8 Hartree energy cutoff ("short") were used, based on DFT BH-LYP results.[71] BH-LYP D3(BJ) dispersion corrections[66] addition were necessary to obtain a bound

ground state.[29,51] The execution driver written by Crespo-Otero and Barbatti[72] was used to run calculations. Only two excitations were allowed in the construction of the reference active space used in DFT/MRCI, and the number of orbitals and electrons were chosen analyzing the impact of increasing it in size on excited-state energies. An (8,8) reference active space was found to be sufficient for DFT/MRCI (see Tables SI-SII in the Supplementary Material). Both basis sets def2-SVP and def2-SV(P)[73] were used in S_0 and S_1 optimizations. Results with the latter basis were used to explore excited states in vertical excitations.

LC-TD-DFTB2 calculations were carried out using a development version of the DFTB+ program package.[74] The ob2-1-1-base[75] Slater Koster (SK) set was used for LC-TD-DFTB2 calculations and the 3ob-3-1[76] SK set for DFTB3 ones, along with a dispersion correction of Lennard-Jones form[77] with universal force field (UFF) parameters.[78] TheoDORE[32–34] was used to calculate CT value and omega matrix for each state. Images of the molecules were created with Jmol.[79]

Due to previous results concluding that basis set superposition error (BSSE) corrections should not be used with small basis sets for stacked dimers,[80] these corrections were not applied in the present study.

III. RESULTS AND DISCUSSION

A. S_0 and S_1 optimized dimer geometries

Dimer structures were optimized using the def2-SVP basis set and the methods displayed in **TABLE** I. Results were classified according to the structures obtained, as shown in **FIG.** 1. for the ground state. A T-shaped-type geometry was also included due to its particular importance in the tetracene crystal phase. Other geometries are identified by the acronyms Rot, PD, and DS, which stand for, respectively, rotated, parallel displaced (consistent with previous studies[26]), and displaced stacked. The state used to optimize the respective geometry is identified following the acronym (e.g., Rot1-S_0 or PD1-S_1).

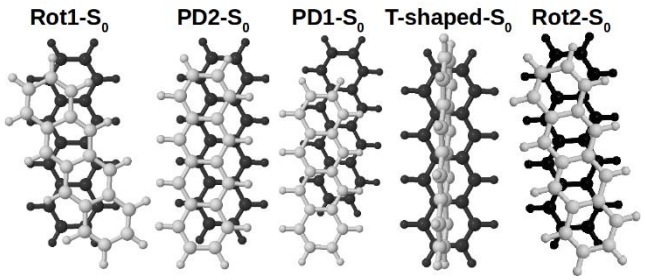

FIG. 1. Relevant optimized geometries obtained for a tetracene dimer in the ground state with SOS-MP2 and def2-SVP basis set. Relative energy increases from left to right (TABLE I). LC-DFTB2 Rot2-S_0 geometry was also included.

TABLE I. Relative energies (kcal/mol) of S_0 minimum geometries for the tetracene dimer, with def2-SVP basis. If the conformation type changed during optimization, the final geometry is indicated.

Optimized geometries	Relative energy of S_0 optimized geometries (kcal/mol)				
	ωB97X-D	**SOS-MP2**	**CAM-B3LYP**	**LC-DFTB2***	**DFTB3***
Rot1-S_0	0.00	0.00	0.00	0.00	0.00
Rot2-S_0	Rot1-S_0	Rot1-S_0	Rot1-S_0	-0.02	0.05
T-shaped-S_0	PD2-S_0	6.25	DS1-S_1 type**	Rot2-S_0	Rot2-S_0
PD2-S_0	0.82	1.04	0.93	0.03	0.11
PD1-S_0	PD2-S_0	3.03	2.62	PD2-S_0	PD2-S_0

* Frequencies were not calculated. ** It has a small imaginary frequency (close to 20*i* cm^{-1}).

TABLE II. Geometrical parameters for S_0 and S_1 optimized geometries of the tetracene dimer. D is the distance between the centers-of-mass of each monomer. The angles α and β and the dihedral angle γ are defined in **FIG.** 2.

Optimized Geometry	Geometrical parameters															
	(TD)-ωB97X-D				**SOS-MP2/SOS-ADC(2)**				**(TD)-CAM-B3LYP**				**LC-(TD-)DFTB2**			
	α (°)	**β (°)**	**D (Å)**	**γ (°)**	**α (°)**	**β (°)**	**D (Å)**	**γ (°)**	**α (°)**	**β (°)**	**D (Å)**	**γ (°)**	**α (°)**	**β (°)**	**D (Å)**	**γ (°)**

Rot1-S_0	179.1	96.1	3.48	21.9	179.7	94.8	3.44	21.9	179.3	93.8	3.52	22.7	178.7	91.8	3.49	18.6
Rot2-S_0		-				-				-			179.0	90.0	3.60	10.7
T-shaped-S_0		-			178.9	176.0	4.99	-1.3		-				-		
PD2-S_0	179.7	107.4	3.73	0.1	178.7	106.1	3.68	0.1	179.7	108.2	3.79	0.1	179.8	82.3	3.62	0.0
PD1-S_0		-			178.2	104.5	4.67	1.5	177.3	107.4	4.58	-0.1		-		
DS1-S_1	177.0	101.5	3.33	0.0	175.8	103.9	3.26	0.0	176.0	103.4	3.33	-0.1	174.0	89.7	3.19	0.0
PD1-S_1	179.0	97.7	4.00	-0.1	177.4	100.6	3.91	0.6	178.6	97.6	4.04	-0.1	173.5	89.9	4.05	0.3

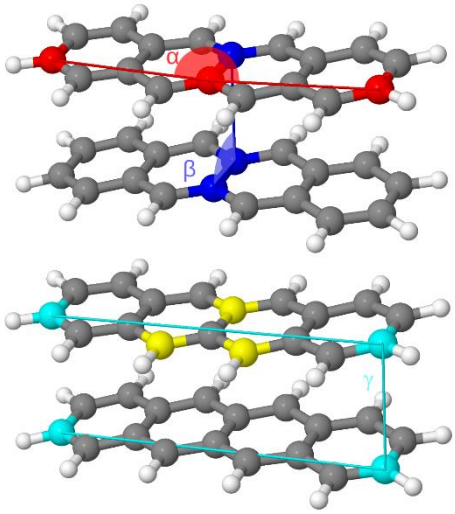

FIG. 2. Atoms used to define relevant geometrical parameters: angles α (red) and β (blue) and dihedral angle γ (cyan). The yellow atoms were used to construct the PECs discussed in Section III. C.

All methods, except LC-DFTB2, consistently predict the lowest S_0 minimum to be the rotated type conformer denoted Rot1-S_0 (**TABLE** I and **FIG.** 1), in which both monomers are parallel, and a non-zero angle is held between their long axes (**TABLE** II). This finding is also consistent with theoretical and experimental results reported by Schouder et al.[26] LC-DFTB2 predicts two nearly degenerate rotated type minima, Rot1-S_0, with intermonomer dihedral close to 19° and consistent with the other methods,

and Rot2-S_0 with a smaller dihedral (close to 11°), the latter with energy lower by only 0.02 eV. This Rot2-S_0 geometry converges at SOS-MP2, CAM-B3LYP, and ωB97X-D to the Rot1-S_0 minimum (**TABLE** I). At SOS-MP2 level, other S_0 minima are predicted to have higher energies, which rises with the decreasing alignment of aromatic rings: PD2-S_0, PD1-S_0, and T-shaped-S_0. This order is also reflected in the interaction energies (**TABLE** III). CAM-B3LYP and ωB97X-D predict similar conformers and relative energies in several cases, including the lowest S_0 minimum, although some conformations, such as the T-shaped-S_0, were predicted not to have minima.

Comparison with SOS-MP2 PD1-S_0 and T-shaped-S_0 geometries suggests that both LC-DFTB2 and DFTB3 lack appreciable minima in these conformations. These two methods also predict nearly degenerate PD2-S_0, Rot1-S_0, and Rot2-S_0 optimized geometries, disagreeing with numerical values predicted by other methods.

The predicted lowest energy S_0 minimum geometry for the tetracene dimer, rotated type, is consistent with previous results based on experiments and DFT optimizations,[26] and on force-field calculations.[81] The stability order of other S_0 minima in **TABLE** I (PD2-S_0, PD1-S_0, and T-shaped-S_0) is also consistent with previous studies of naphthalene, anthracene, and tetracene dimers.[82–84] SOS-MP2 PD2-S_0 interaction energy (**TABLE** III) agrees with the SOS-MP2/def2-TZVP value for a similar configuration reported by Silva et al.[27] Spillebout et al.[16] argued that a C_2 geometry (rotated similar to Rot1-S_0) is unstable for tetracene and pentacene dimers based on ωB97X-D/6-311G vibrational frequencies, whereas a PD2-S_0 type geometry is a minimum. However, these results for the Rot1-S_0 are not in agreement with the ones presented in this study or those reported by Schouder et al.[26]

TABLE III**.** Interaction energies for S_0 optimized geometries of the tetracene dimer (kcal/mol).

Method	Interaction energy (kcal/mol)			
	Rot1-S_0	**PD2-S_0**	**PD1-S_0 #**	**T-shaped-S_0 #**

SOS-MP2	-16.93	-15.89	-13.90	-10.68
ωB97X-D	-20.42	-19.60	-	-
CAM-B3LYP	-17.62	-16.69	-15.00	-
LC-DFTB2	-18.87	-18.75	-14.67	-10.10

SOS-MP2 geometries were used for LC-DFTB2, as no minima were predicted with the latter (see **TABLE** I)

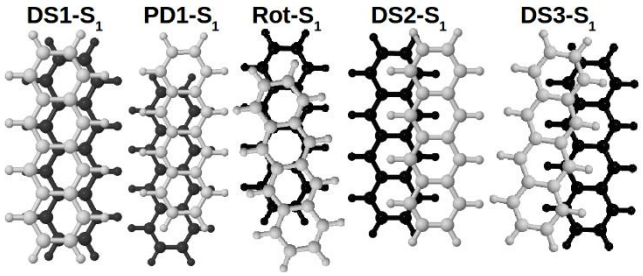

FIG. 3**.** Relevant optimized geometries obtained for a tetracene dimer in the first excited state with SOS-ADC(2) and def2-SVP basis set. Relative energies increase from left to right (**TABLE** IV). The TD-CAM-B3LYP DS2-S_1 and TD-ωB97X-D DS3-S_1 geometries were also included.

TABLE IV**.** Relative energies (kcal/mol) for the S_1 optimized geometries of the tetracene dimer, with def2-SVP basis set unless stated otherwise. If the conformation type changed during optimization, the final geometry is indicated.

Optimized geometries	**Relative energy of S_1 optimized geometries (kcal/mol)**			
	ωB97X-D	**SOS-ADC(2)**	**CAM-B3LYP**	**LC-TD-DFTB2**
DS1-S_1	0.00	0.00	0.00	0.00
PD1-S_1	3.19	3.15	2.52	3.00
Rot1-S_0*	PD1-S_1	4.35 Rot-S_1	PD1-S_1	DS1-S_1
T-shaped-S_0*	9.78 DS3-S_1**	17.89	9.56 DS2-S_1	DS1-S_1

* Calculations were done with def2-SV(P). Frequencies were not calculated.

** Intermonomer dihedral γ close to 7°.

Concerning the excited state, all methods predicted a consistent lowest energy minimum (DS1-S_1, see **TABLE** IV and **FIG.** 3), similar to a D_{2h} stacked model, but with one monomer displaced along its shorter axis (see **TABLE** II). Regarding other conformations, PD1-S_1 was consistently predicted as a higher energy minimum by all methods. Rot1-S_0 and T-shaped-S_0 conformers were also optimized for S_1, and in all cases, the conformation either changed to PD1-S_1, DS1-S_1, or conformers with higher relative energy (greater than 4 kcal/mol, **TABLE** IV). Hence, among the calculated geometries, only the DS1-S_1 should be a relevant minimum geometry in the S_1 state. Particularly at SOS-ADC(2) level, the Rot1-S_0 initial conformation converged to a different rotated conformer (Rot-S_1), with an intermonomer dihedral angle close to 10° instead of 20-22°.

The DS1-S_1 geometry should be sufficiently close to an eclipsed geometry to allow the latter to be reached, should it be more stable. However, given the relevance of eclipsed D_{2h} structure for aromatic excimers,[38,42] besides parallel displaced ones,[21] two additional geometries were considered. An eclipsed D_{2h} geometry and a parallel displaced one with one monomer slipped by 0.05 Å in the long and short axis (denoted DS4-S_1). After optimization, SOS-ADC(2)/def2-SV(P) predicts the D_{2h} energy to be higher by 2.2 kcal/mol relative to DS1-S_1, and the DS4-S_1 structure (C_1 symmetry) to converge to the DS1-S_1 geometry. Concerning TDDFT calculations using the levels ωB97X-D/def2-SV(P) and CAM-B3LYP/def2-SVP, the eclipsed D_{2h} structure was higher in energy by 0.37 kcal/mol and 0.20 kcal/mol, respectively, than the DS1-S_1 structure, suggesting a flatter potential energy surface relative to SOS-ADC(2). The DS4-S_1 structure converged to a geometry similar to the optimized D2h for CAM-B3LYP, and to the DS1-S_1 minimum for ωB97X-D. In all tested cases, the DS1-S_1 was still the lowest S_1 energy geometry obtained.

B. Dimer Vertical Excitations at Optimized Geometries

Vertical excitations for the dimer were calculated with the def2-SV(P) at the S_0 and S_1 minima optimized with the same basis set. The latter geometries were very similar to def2-SVP optimized ones (**TABLE** I and **TABLE** IV, **FIG.** 1 and **FIG.** 3). Results for the monomer at SOS-MP2/def2-SV(P) S_0 optimized geometry were also included for comparison. Excitation energies, symmetries, and oscillator strengths are also shown in Tables SIII-SVII.

TABLE V**.** Excitation energy (EE, eV) and oscillator strength (*f*) for the ^1L_a and ^1L_b states of the tetracene monomer. SOS-MP2/def2-SV(P) optimized geometry was used for all calculations.

Method	^1L_a (1^1B_{2u})		^1L_b (1^1B_{3u})	
	EE (eV)	***f***	**EE (eV)**	***f***
DFT/MRCI	2.69 2.74[a]	0.127 0.109[a]	3.27 3.22[a]	0.004 0.002[a]
SOS-ADC(2)	3.33	0.111	3.50	0.001
ADC(2)	3.07	0.101	3.59	0.001
TD-ωB97X-D	2.88	0.087	3.71	0.003
LC-TD-DFTB2	3.03	0.113	4.01	0.191
CASPT2[b]	2.79	0.125	3.15	0.004
Experimental	2.71[c] 2.60[d]	-	3.32[c] 3.14[d]	-

[a] Reference[85]. [b] Reference[86]. [c]Reference[87]. [d]Reference[88].

Regarding the monomer (**TABLE** V), DFT/MRCI predicts excitation energies of 2.69 and 3.27 eV for 1^1B_{2u} and 1^1B_{3u} states, in excellent agreement with experimental results[87,88] and previously reported calculations with DFT/MRCI,[85] using both SV(P) and TZVP basis sets, and CASPT2.[86] Other methods predict higher excitation energies for both states and a varying energy gap between them, such as 0.17 eV [SOS-ADC(2)] and 0.98 eV (LC-TD-DFTB2). In particular, SOS-ADC(2) has the highest overestimation of ^1L_a, but the closest prediction of ^1L_b relative to experimental results, among the single-

reference methods. Excepting LC-TD-DFTB2, all methods predict a bright S_1 state and a S_2 with small, but non-zero oscillator strength for the monomer (**TABLE** V), which agrees with the experiments.[88]

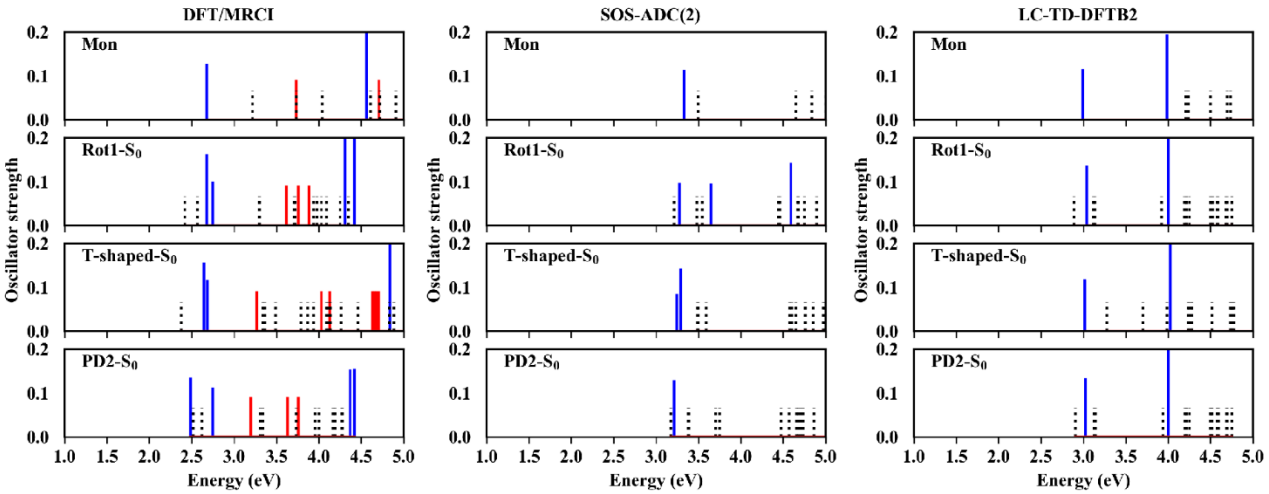

FIG. 4. Excitation energies and oscillator strengths for the tetracene monomer (Mon) and dimer S_0 optimized geometries (**FIG.** 1). Bright singly excited ($f > 0.05$), dark singly excited, and doubly excited states are represented by solid blue, dotted black, and solid red lines, respectively. The height is proportional to the oscillator strengths for the bright states and fixed for the others. LC-DFTB2 Mon, Rot1-S_0, and PD2-S_0 geometries were used for LC-TD-DFTB2, and SOS-MP2 geometries in all other cases. Fig. S1 contains all methods used.

There is an overall good agreement among dimer spectra using different methods (**FIG.** 4 and **FIG.** 5). Focusing on S_1-S_4 states for all geometries, we see that other methods predict higher excitation energies relative to DFT/MRCI, particularly SOS-ADC(2). This general pattern could be partly due to the monomer itself, as it also appears for the S_1 and S_2 states of the latter (**TABLE** V). For the S_0 minimum dimer geometries investigated — Rot1-S_0, T-shaped-S_0, PD2-S_0 — all methods predict a bright

state to be either S_1 or within 0.3 eV of it (**FIG.** 4). DFT/MRCI predicts a dark S_1 state for all geometries except PD2-S_0, where the S_2 dark state is nearly degenerate with the S_1 bright state (**FIG.** 4). Other methods follow closely, except for the T-shaped-S_0 geometry, where a bright S_1 state, similar in energy to the monomer bright S_1 state, is predicted by SOS-ADC(2) and LC-TD-DFTB2 (**FIG.** 4). The excimer geometry, DS1-S_1 conformer, presents a rather distinct picture as all methods predict the stabilization of the first dark state, which is lower by at least 1.0 eV compared to other singly excited states, including the first bright state (**FIG.** 5).

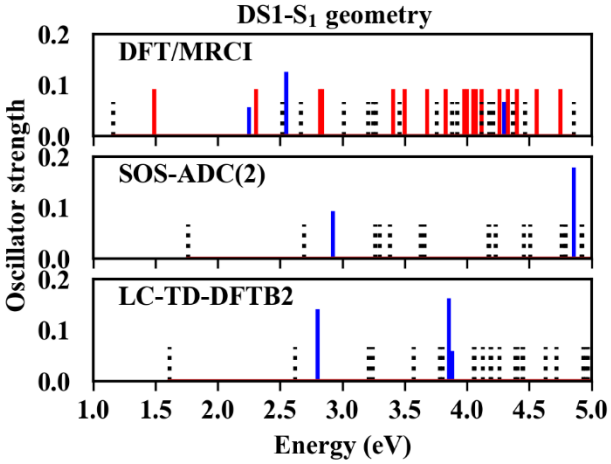

FIG. 5. Same as **FIG.** 4, but focusing on DS1-S_1 optimized geometry (**FIG.** 3) and varying the method. Bright singly excited (f > 0.05), dark singly excited, and doubly excited states are represented by solid blue, dotted black, and solid red lines, respectively. DFT/MRCI calculations used SOS-ADC(2) geometry. SOS-ADC(2) and LC-TD-DFTB2 used geometries optimized at the same level. Fig. S2 contains all methods used.

Current implementations of TDDFT and TD-DFTB cannot predict doubly excited states (due to the adiabatic approximation of the time-dependent correlation-exchange potential[89]); neither can ADC(2) (due to the expansion of the 2p-2h matrix elements only to the zeroth order of perturbation theory[48]).

Because at the Rot1-S_0, PD2-S_0, and T-shaped-S_0 geometries, DFT/MRCI predicts doubly excited states much higher than S_1 (by 1.0 eV or more) and at least 0.5 higher than the first bright states (**FIG.** 4), TDDFT, TD-DFTB, and ADC(2) can be applied to describe the absorption spectrum without a problem. However, at the excimer geometry, DS1-S_1, a low-lying doubly excited state is predicted to be only 0.4 eV above the S_1 state and located lower than the first bright state (**FIG.** 5). Hence, this state is expected to become important for excimer formation and survival, limiting the applicability of these methods. Previous studies also reported the existence of a low-lying doubly excited state for the tetracene dimer[7,8] and related systems such as pentacene[7,90] and covalently linked tetracene dimers.[23]

Regarding comparison to experimental data for the tetracene dimer in solution, Katul and Zahlan[24] reported the first absorption maximum close to 2.3 eV, and Iannone and Scott[25] reported a similar value (close to 475 nm, 2.6 eV) for a tetracene dimer in a solid host matrix. These values are consistent with the first and second DFT/MRCI bright states (f > 0.05) for all three S_0 optimized geometries (**FIG.** 4, **TABLE** VI): S_3 (2.68 eV) and S_4 (2.75 eV) at Rot1-S_0, S_1 (2.49 eV) and S_4 (2.75 eV) at PD2-S_0, and S_2 (2.64 eV) and S_3 (2.69 eV) at T-shaped-S_0. Since the latter geometry has relative energy much higher than the others, it is unlikely to contribute, but PD2-S_0 conformer is higher by near 1 kcal/mol at SOS-MP2/def2-SV(P) level (**TABLE** I), and it could be populated if the temperature is high enough. Other methods predict a first aborption maximum at energies higher than DFT/MRCI by 0.16-0.72 eV (**TABLE** VI). The fluorescence spectrum of tetracene dimers trapped in a poly(methyl methacrylate) matrix shows a broad band, which has a peak maximum at 2.2 eV, another peak at 2.1 eV, and a weak shoulder at 1.9 eV, as reported by Iannone and Scott.[25]. Comparison with these results shows that our vertical emission energies are lower, ranging between 1.16 eV (DFT/MRCI) and 1.77 eV(SOS-ADC(2) (**TABLE** VI). From shifts in the fluorescence excitation spectra between monomer and dimer of 250 cm^{-1} and the experimental Stokes shift of 300 cm^{-1}, Iannone and Scott estimate the tetracene pair separation to lie between 4 to 8 Å in the matrix. The weaker interaction in this case as compared to the one in the present

dimer with a distance of 3.26 Å might be one reason for the discrepancies between calculated and experimental emission energies, in addition to deficiencies of the computational methods.

TABLE VI. Excitation energy (eV) for relevant states of the tetracene dimer for the processes considered. For the absorption, the first two bright states ($f > 0.05$) are included for both Rot1-S_0 and PD2-S_0 geometries. The adiabatic state is indicated in parenthesis. For the emission, the S_1 state at DS1-S_1 geometry is included.

Process	Geometry	Relevant state	Method					Experimental
			DFT/MRCI	SOS-ADC(2)	ADC(2)	TD-ωB97X-D	LC-TD-DFTB2	
Absorption	Rot1-S_0	First bright	2.68 (S_3)	3.28 (S_2)	2.93 (S_1)	2.97 (S_2)	3.04 (S_2)	2.3[a]-2.6[b]
		Second bright	2.75 (S_4)	3.65 (S_6)	3.13 (S_4)	3.27 (S_4)	4.00 (S_6)	
	PD2-S_0	First bright	2.49 (S_1)	3.21 (S_2)	2.87 (S_1)	2.91 (S_2)	3.04 (S_2)	
		Second bright	2.75 (S_4)	-	3.14 (S_4)	-	4.00 (S_6)	
Emission	DS1-S_1	S_1	1.16	1.77	1.42	1.56	1.62	1.9-2.2[b]

[a] Reference[24]. [b] Reference [25].

Besides the general overview of the spectra, it is also important to compare the particular nature of states among methods. Oscillator strengths, symmetries, omega matrices, and CT values for low-lying states (S_1-S_4) were employed to identify analogous states among methods. Omega matrices and CT values require defining proper fragments, and we used two schemes here (Fig. S3). To calculate CT values, we considered each monomer as a fragment, such that the CT descriptor quantifies intermonomer charge-transfer interactions. To calculate omega matrices, we used a more detailed grid. Each carbon was defined as a fragment, and, in the dimer case, the first half of the fragments belongs to a monomer, while the second half to the other. Hydrogen atoms were included in the fragment of the respective bonded carbon. Examples of omega matrices are shown in **FIG.** 6. Each cell specifies the weight of a given charge-transfer for the excitation considered, and the respective line and column specify the

number, with origin at the lower left corner, of the two fragments involved (provided they are not equal).[32]

With this fragmentation scheme, each omega matrix for the dimer can be divided into four groups of fragments: upper left and lower right ("diagonal" blocks), and upper right and lower left ("off-diagonal" blocks). For two dominant off-diagonal blocks (such as in S_2 state at Rot1-S_0 in **FIG.** 6), both the electron and the hole are on the same monomer (excitonic resonance states), whereas for two dominant diagonal blocks (as in S_1 state at Rot1-S_0 in **FIG.** 6) they are separated on different monomers (charge-resonance (CR) states).[32] If a single diagonal block is dominant (such as in S_2 at T-shape-S_0 geometry in **FIG.** 7), then the exciton is localized on a single monomer, and the state is locally excited.[32] A single dominant off-diagonal block corresponds to a charge-transfer (CT) state (exemplified by S_1 state at T-shape-S_0 geometry in **FIG.** 7).[32] Lastly, equal contributions from all four blocks characterizes a mixed state (for example, S1 at PD2-S_0 in **FIG.** 7). Omega matrices for the tetracene monomer and selected dimer geometries are included in the supporting information (Figs. S4-S8) for all methods used, along with CT value (Table SVIII), oscillator strength, and symmetry for each excited state (Tables SIII-SVII).

TABLE VII**.** Excitation energies (EE), irreducible representation of the C_2 group (sym), and oscillator strengths (*f*) for the Rot1-S_0 geometry (**FIG.** 1). A lower-case letter beside each energy identifies analogous states among methods. Tables SIII-SVII present further data for all calculated geometries.

State	DFT/MRCI			SOS-ADC(2)			LC-TD-DFTB2		
	EE (eV)	*f*	sym	EE (eV)	*f*	sym	EE (eV)	*f*	sym
S_1	2.42 a	0.015	A	3.21 b	0.003	B	2.89 b	0.004	B
S_2	2.57 b	0.005	B	3.28 c	0.095	A	3.04 c	0.134	A
S_3	2.68 c	0.159	A	3.48	0.014	A	3.12 a	0.020	A
S_4	2.75 d	0.098	B	3.48	0.010	B	3.14 d	0.006	B

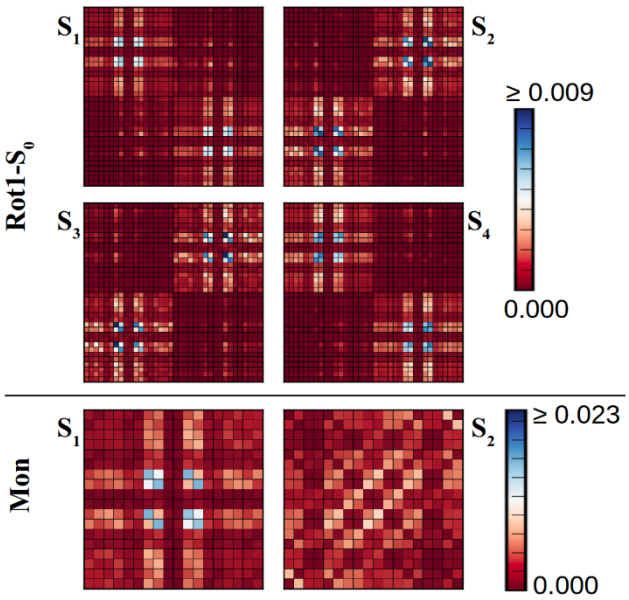

FIG. 6. S_1-S_4 DFT/MRCI omega matrices for tetracene dimer at Rot1-S_0 geometry. For comparison, S_1 and S_2 DFT/MRCI omega matrices for the monomer (Mon) are also shown. The complete set of omega matrices is shown in Figs. S4-S8.

Using these tools, we see that the order of analogous states varies with the method, as shown in **TABLE** VII for the Rot1-S_0 geometry (Tables SIII-SVII for all). However, for a given method, these inversions in the order of states are, in most cases, associated with states with relatively small energy differences (< 0.4 eV), suggesting a general agreement among methods. Concerning oscillator strengths, there is a good agreement among methods for all geometries regarding the identification of each state as bright (f > 0.05) or dark, as can be seen in **FIG.** 4 and **FIG.** 5. Analyzing the S_1 state for the T-shaped-S_0 structure, one can see from Tables SVI (lowercase letters besides excitation energies label comparable states) and SVIII, that the S_1 state (1^1B_1) for DFT/MRCI and ADC(2) has a pronounced CT character and a smaller oscillator strength whereas the 2^1B_1 state has a smaller CT character and a larger oscillator strength. For the other methods, this situation is inversed (for SOS-ADC(2) the 2^1B_1 CT value is 0.89 e, not included in Table SVIII). This inversion in the order of analogous states (1 $^1B_1$ and 2 $^1B_1$) among

different methods still seems acceptable, however, in view of the relatively small energy difference between these two states (0.22-0.35 eV for all methods).

Omega matrices (**FIG.** 6 to **FIG.** 8) provide further information, as they can be used to assign the state character as CT, CR, excitonic, localized, or mixed.[32] At Rot1-S_0 geometry (**FIG.** 6), S_1 to S_4 states are connected to the S_1 state of the monomer, as shown by the patterns of the respective dimer omega matrices. The main patterns of the omega matrices for states S_2 and S_3 are located on the off-diagonal blocks showing an excitonic resonance character. On the other hand, S_1 and S_4 states are of charge resonance character as the diagonal blocks, connected to intermonomer interactions, are dominant in this case. CT values confirm this picture, as they are small for S_2 and S_3 (CT < 0.15), and large for S_1 and S_4 (CT > 0.8). This situation is similar to the Frenkel models describing dimer states as combinations of monomer states,[91] and the relevant role of charge-transfer interactions is consistent with a previous work that demonstrated that the inclusion of a charge-transfer type of coupling in the Holstein Hamiltonian is necessary to describe experimental results in a tetracene crystal.[22]

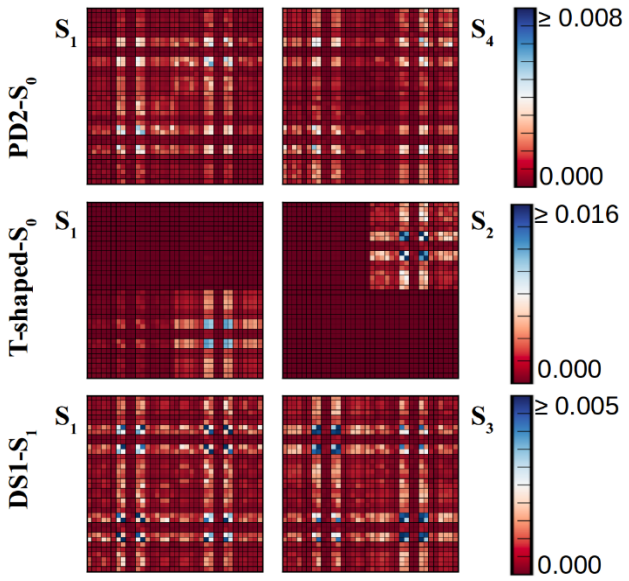

FIG. 7. DFT/MRCI omega matrices for tetracene dimer at geometries PD2-S_0, T-shaped-S_0, and DS1-S_1. The complete set of omega matrices is shown in Figs. S6-S8.

DFT/MRCI predicts a more complex scenario for the other geometries. At the PD2-S_0 geometry, S_1 and S_4 are predicted to be mixed states (**FIG.** 7), and for the T-shaped-S_0 (**FIG.** 7), S_1 is a CT state, S_2 and S_3 (**Fig. S8**) are almost degenerate excitations localized at each monomer, and S_4 is a doubly excited state. At DS1-S_1 geometry, all S_1-S_4 DFT/MRCI states are predicted to be either of mixed (S_1 and S_3, **FIG.** 7) or doubly excited character (S_2 and S_4). For the S_1 state, the DFT/MRCI CT value is quite similar to other methods (Table SVIII), and shows that charge transfer interactions are relevant for the excimer. The splitting among singly excited states for the latter geometry is predicted to be much larger, close to 1 eV (**FIG.** 9), suggesting a stronger interaction between monomers in this geometry. The considerable decrease in the S_1 state energy implies that this splitting is due to the excimer relaxation itself.

Despite the order inversions, LC-TD-DFTB2 predicts similar pictures regarding the nature of states (*e.g.*, CR associated with monomer S_1) and comparable CT values for the singly excited states, exceptions being states S_2 and S_3 at PD2-S_0 (**FIG.** 8), and S_3 at DS1-S_1 geometry. In the latter cases, DFT/MRCI predicts states with more mixed character. In contrast to the other methods, SOS-ADC(2) predicts excitonic states connected to the S_2 state of the monomer (**FIG.** 6) among the low-lying states — S_3 and S_4 at Rot1-S_0 (**FIG.** 8), PD2-S_0 and T-shaped-S_0 — instead of CT/CR, meaning that the latter types of state are destabilized relative to excitonic ones by this method.

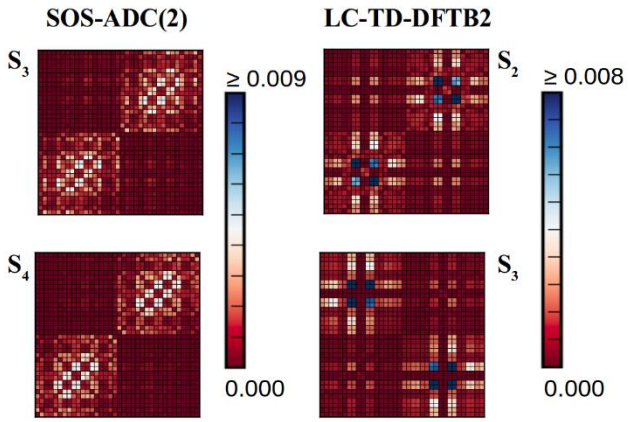

FIG. 8. Tetracene dimer omega matrices for SOS-ADC(2) at Rot1-S_0 geometry, and LC-TD-DFTB2 at PD2-S_0 geometry. The complete set of omega matrices is shown in Figs. S4-S8.

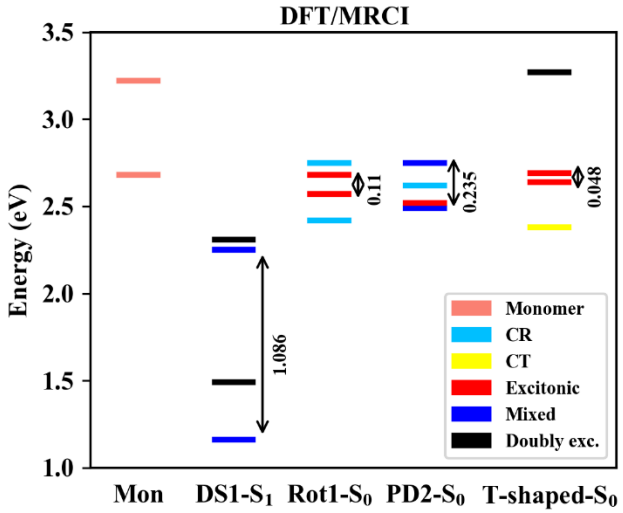

FIG. 9. DFT/MRCI vertical excitations for each tetracene dimer geometry and the monomer (Mon). S_1 and S_2 states are represented for the monomer and S_1 to S_4 for the dimer. The nature of the state is represented by the line color. CR and CT stand for charge resonance and charge transfer, respectively. Mixed states have relevant contributions from both excitonic and charge-transfer interactions.

Energy level diagrams are shown in **FIG.** 9 for DFT/MRCI S_1-S_4 states with the splitting of states of similar character, summarizing the previous discussion based on **FIG.** 6 to **FIG.** 8. In the case of vertical

excitations from S_0, excitonic splittings amount to a few tenths of eV. As mentioned earlier, the situation is quite different for the DS1-S_1 geometry, where the corresponding splitting increases to 1 eV, and the two singly-excited states are mixed excitonic and CT states.

C. Potential Energy and Charge-Transfer Curves

Potential energy curves (PECs) were used to analyze the relationship between charge transfer and excimer survival, and its differences among methods. SOS-ADC(2), TD-ωB97X-D, LC-TD-DFTB2, and DFT/MRCI were used. The lowest energy S_1 minimum geometry (DS1-S_1, **FIG.** 3) was taken as the starting point. For DFT/MRCI and LC-TD-DFTB2, the SOS-ADC(2) optimized geometry was used. To construct the PEC, one monomer was rigidly displaced along the normal vector of the plane defined by the three yellow atoms in **FIG.** 2, whereas the other monomer was kept fixed. Symmetry labels were used to identify states, except for LC-TD-DFTB2, since orbitals for the latter method became localized to each monomer, for large intermonomer distances.

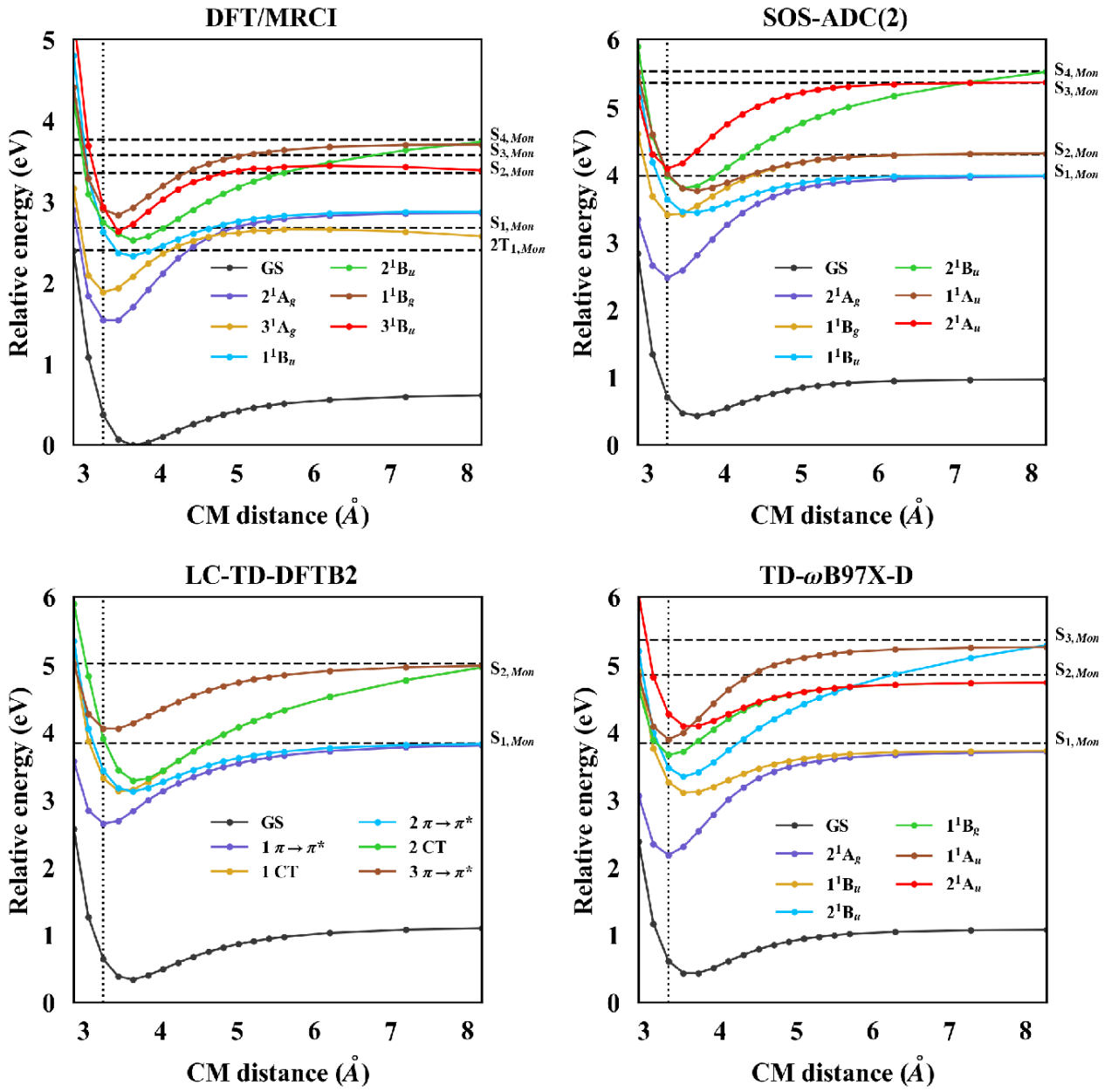

FIG. 10: Diabatically connected PEC along the intermonomer distance for the tetracene dimer. Energies are relative to the Rot1-S_0 minimum, except for DFT/MRCI, for which the lowest value of the S_0 energy (3.65 Å) was used as a reference. The DS1-S_1 optimized geometry is marked with a dotted vertical line. The excited states of the monomer (*Mon*) are represented as horizontal lines. In LC-TD-DFTB2 case, states were labeled based on their character, as symmetry labels were not applicable.

TABLE VIII**.** Dissociation energy (D_e, eV) for each state. The DFT/MRCI S_1 to S_4 states at the DS1-S_1 geometry were included. CT and doubly excited (DE) states were not included. The lower-case letter besides each value is used to mark analogous states.

Method	State			
	S_1^*	S_2^*	S_3^*	S_4^*
DFT/MRCI	1.32 a	DE	0.54 c	DE/CT
SOS-ADC(2)	1.49 a	0.90 b	0.55 c	CT d
TD-ωB97X-D	1.52 a	0.62 c	CT d	1.07 b
LC-TD-DFTB2	1.16 a	CT d	0.7 c	CT b

* the state number refers to DFT/MRCI at DS1-S_1 geometry.

As can be seen from **FIG.** 10, all single-reference methods predict a similar general profile relative to DFT/MRCI, but relevant differences are found, such as a shallower S_1 state minimum (2^1A_g for all methods) and smaller energy gaps between states S_2-S_4 in LC-TD-DFTB2. Among the singly excited states, the description of the most analogous states is quite similar, as shown by the dissociation energies in **TABLE** VIII. Excimer stabilization energies for the S_1 state also agree quite well among single-reference methods (**TABLE** IX). The most important difference of single-reference methods relative to DFT/MRCI is the low-lying doubly excited state (3^1A_g) in the latter, which crosses with the state associated with the excimer (2^1A_g), and could lead to significant deficiencies in the description of photophysical processes by single-reference methods. This crossing is similar to previously reported results for a pentacene dimer.[90] Similarly, a previous study of an intermonomer displacement curve at double spin-flip restricted active space level for two stacked D_{2h} tetracene monomers[8] also reported a low-lying doubly excited ^1A_g state, which becomes nearly degenerate with S_1. As shown in **FIG.** 10, the doubly excited 3^1A_g state has energy near twice the T_1 state energy of the monomer, suggesting it is the state involved in the singlet fission process.

TABLE IX. S_1 excimer stabilization energy (ESE), predicted as the difference between the vertical excitation energy (VE) and adiabatic excitation energy (AE). All values are in eV.

Energy	SOS-ADC(2)	TD-ωB97X-D	TD-CAM-B3LYP	LC-TD-DFTB2
VE	3.21	2.88	3.06	2.89
AE	2.47	2.19	2.30	2.37
ESE	0.74	0.69	0.76	0.52

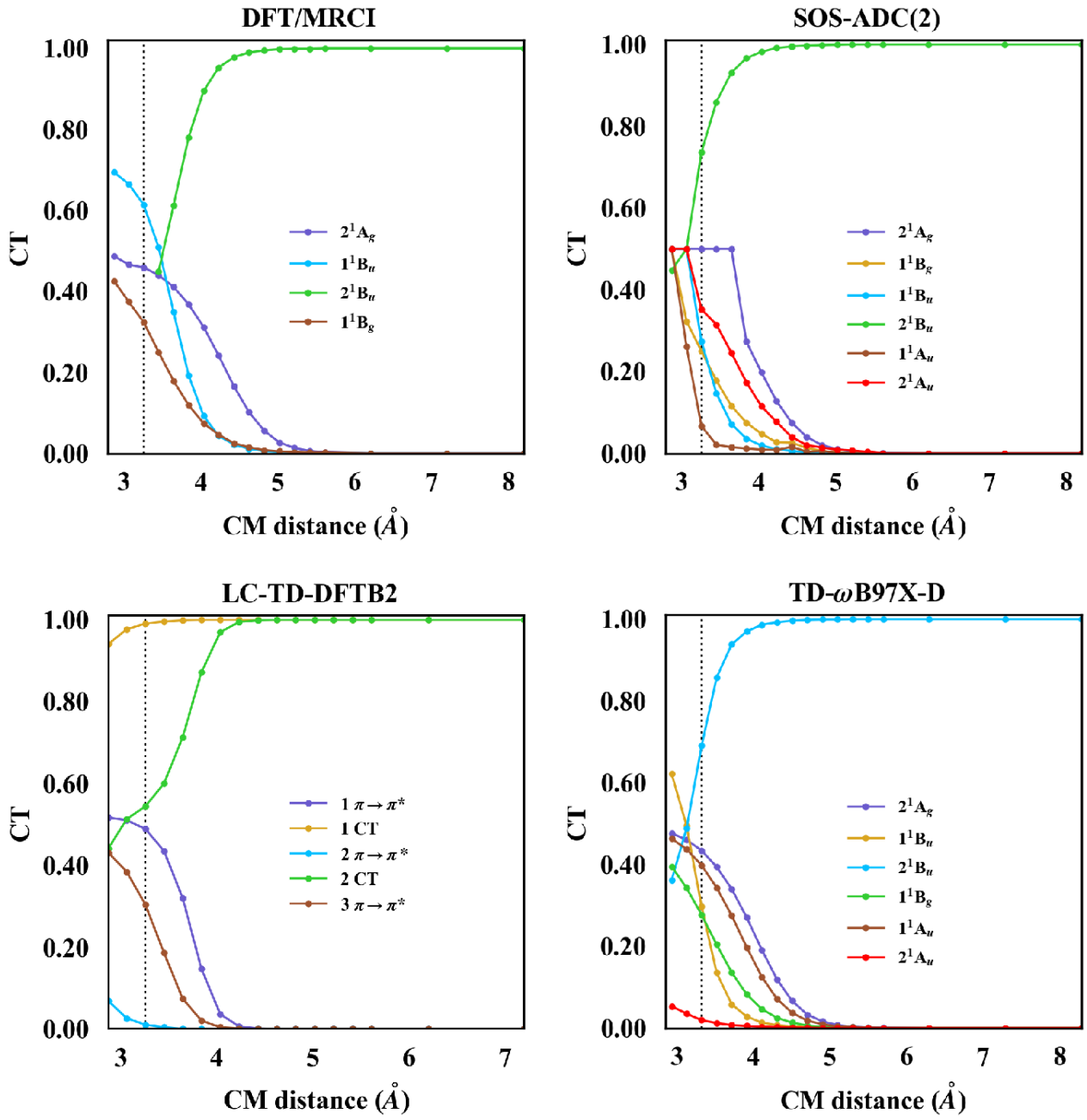

FIG. 11: Diabatically connected CT curves along the intermonomer distance for the tetracene dimer. DS1-S_1 optimized geometry is marked with a dotted vertical line. 3^1A_g and part of the 2^1B_u DFT/MRCI states weres excluded due to the dominant doubly excited character.

Diabatically connected CT values for the PECs in **FIG.** 10 are given in FIG. 11

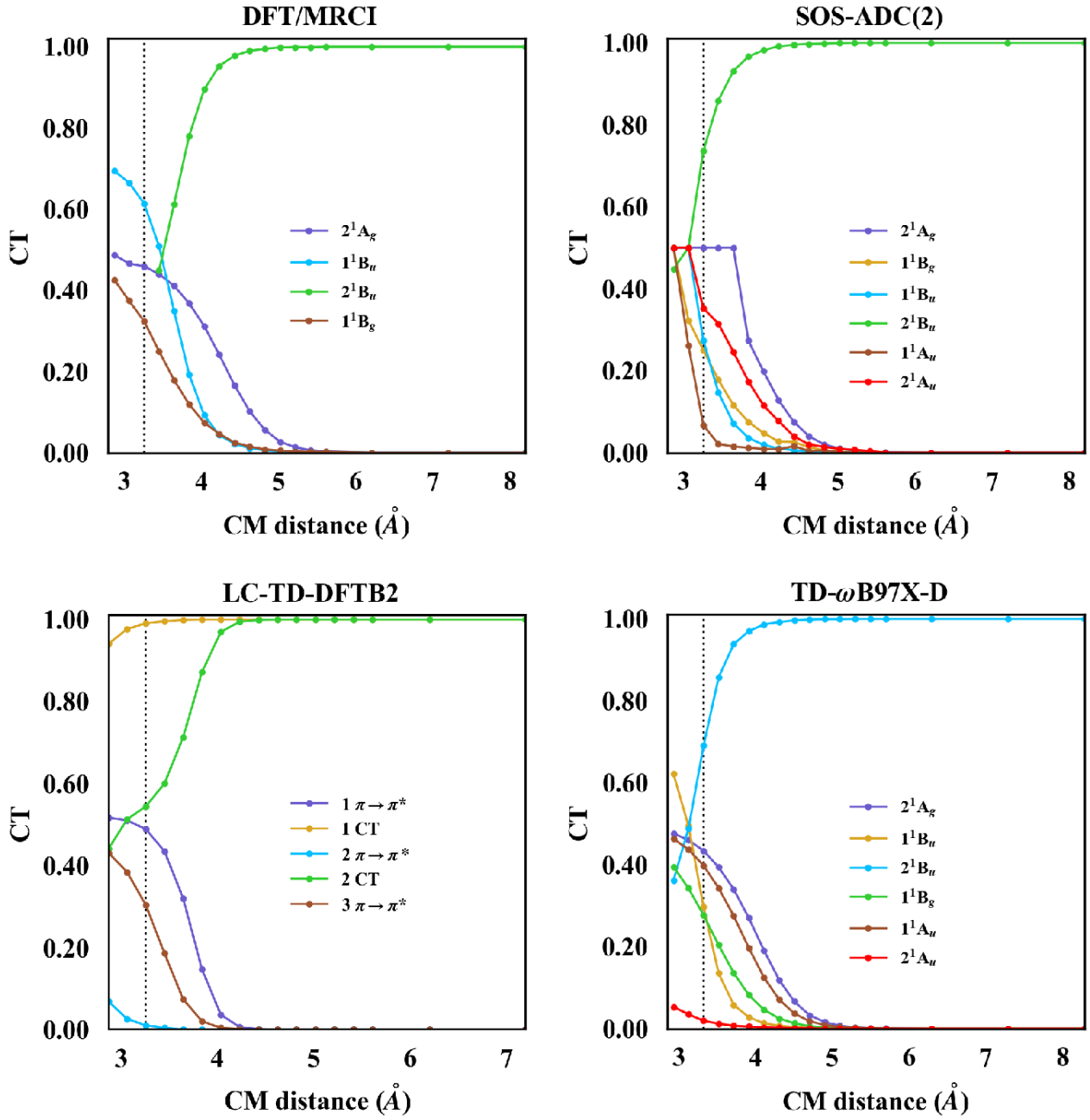

FIG. 11. When analyzed together, PECs and CT values reveal that the decrease of potential energy associated with excimer survival in S_1 mirrors the increase of intermonomer charge transfer, measured by CT values. Excluding CT and doubly excited states, this is also valid for higher-lying states. Focusing on DFT/MRCI, a comparison of the 2^1A_g and 1^1B_u PEC and CT curves suggests that the dissociation energy (D_e) is proportional to the distance upon which charge-transfer interactions vanish (D_{CT}, the point

at which CT becomes very small, e.g., 0.05). This correlation is not always monotonous, however, as exemplified by the 1^1B_g state in the DFT/MRCI curve in **FIG.** 12. Hence, charge-transfer interactions could have a prominant role in the first two states, but not in the latter. Due to the absence of doubly excited states, SOS-ADC(2) presents a clearer picture and corroborates the previous relation, as both D_e and D_{CT} decrease in the order 2^1A_g, 2^1A_u, 1^1B_g, and 1^1B_u, whereas 1^1A_u does not properly fit this tendency (**FIG.** 12). TD-ωB97X-D method presents similar results, although exchanging the roles of 1^1A_u and 2^1A_u. Lastly, the first three $\pi \rightarrow \pi^*$ LC-TD-DFTB2 states also fit this tendency, specifically in the following order: 1 $\pi \rightarrow \pi^*$, 3 $\pi \rightarrow \pi^*$, and 2 $\pi \rightarrow \pi^*$. A similar qualitative relation also appears in previously reported results for the benzene dimer PEC and CT curves,[38] as states with negligible CT values remain unbounded, and states with deeper wells are associated with CT values that vanish at larger intermonomer distances.

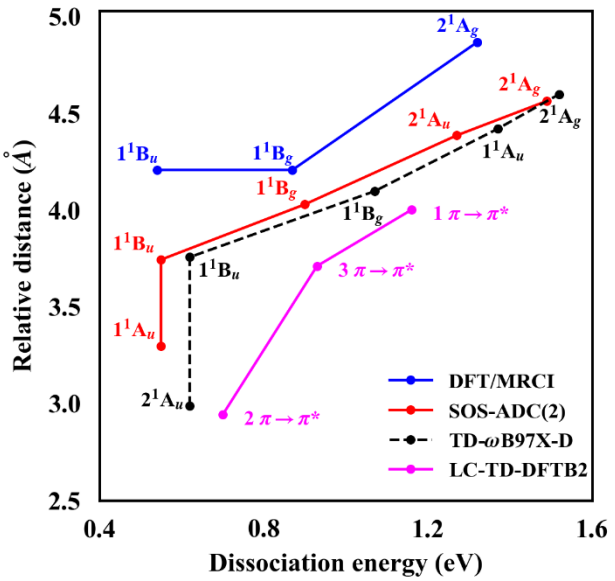

FIG. 12**:** Correlation between relative distance at which the CT curve becomes smaller than 0.05 (FIG.

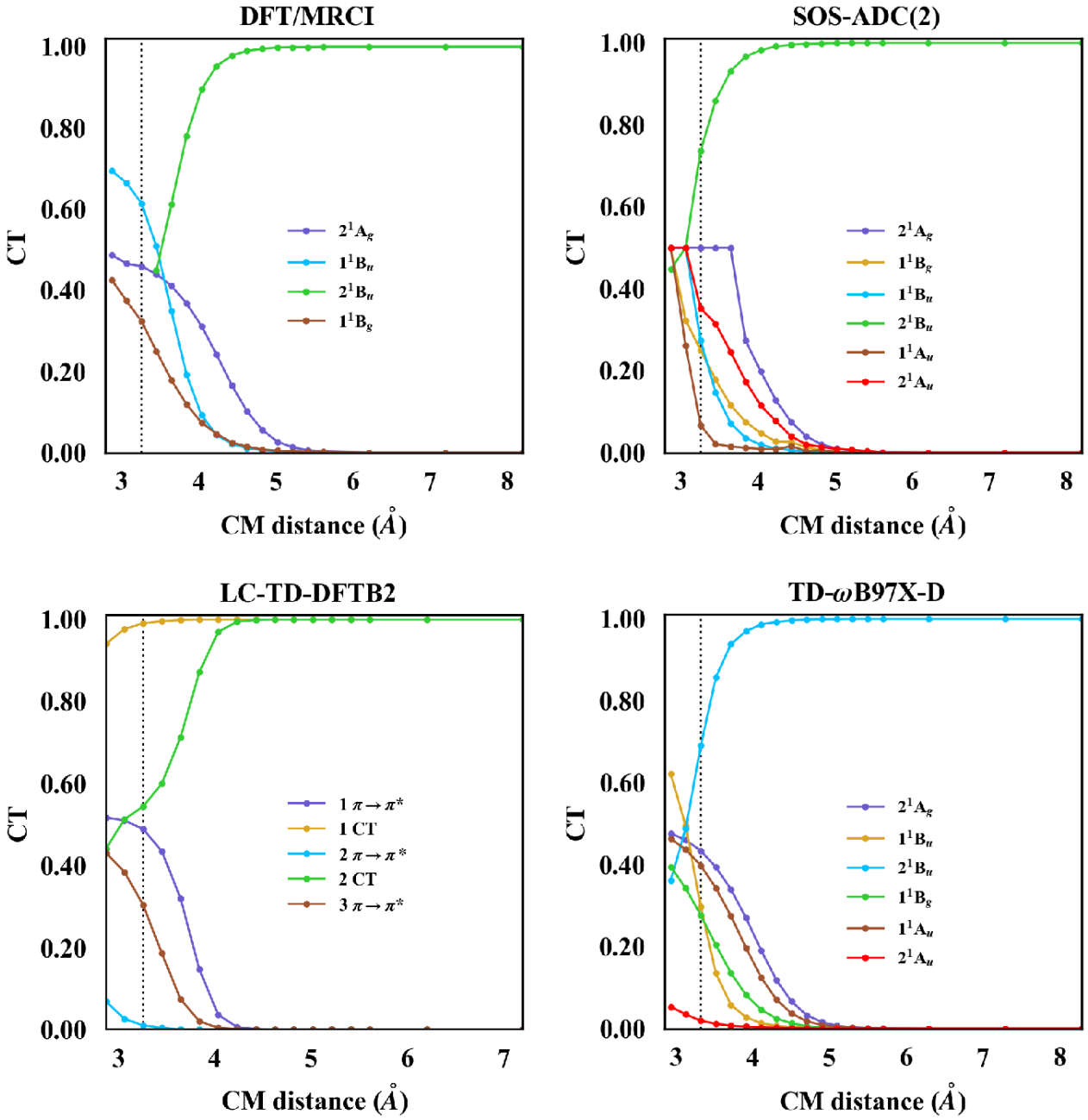

11

FIG. 11) compared to dissociation energy (**FIG.** 10) for each state.

IV. CONCLUSIONS

Benchmark results were reported for the tetracene dimer using single-reference methods and DFT/MRCI. Results of the latter method are consistent with available experimental data for absorption spectra. We predict emission excitation energies for the excimer that are significantly lower than existing experimental data for tetracene dimers that do not present typical excimer behavior. Our calculations suggest that these excitation energies might be useful to differentiate excimer formation from other structural changes between tetracene dimers upon absorption.

Among the tested methods, consistent results were predicted for optimized geometries of S_0 and S_1 states and for the corresponding excitation spectra. Comparison of omega matrices shows that the specific nature of states varies appreciably with dimer geometry. Particularly at the excimer geometry (DS1-S_1), the geometry relaxation leads to a more complex scenario, with low-lying mixed character as well as doubly excited states. The first low-lying doubly excited state has an asymptotic energy value in the potential energy curve consistent with that of two times the energy of the monomer T_1 state, confirming that it is the state connected to singlet fission. This state is also found to cross the state associated with the excimer and becoming the lowest state asymptotically for large intermonomer distances, and, therefore, should be relevant in the singlet fission process. The absence of the doubly excited state can also lead to problems in the description of general excimer related processes by single-reference methods.

LC-TD-DFTB2 provides a good overall description of optimized geometries, associated spectrum, and the nature of low-lying singly excited states, relative to other single-reference methods. Inversions in the order of low-lying states relative to DFT/MRCI and other methods occurred mostly among energetically close states (gaps lower than 0.4 eV). Relative energies of ground-state conformers suggest a flatter potential energy curve relative to SOS-MP2, but excited-state conformers agree quite well with

the prediction of other methods. Hence, LC-TD-DFTB2 should be able to provide a description of the excimer formation and survival processes in line with other single-reference methods.

Results based on PEC and CT curves suggest that charge-transfer interactions are necessary for the excimer stabilization. This could be expressed qualitatively as a relation between the dissociation energy of each state and the associated CT curve vanishing distance. Hence, charge-transfer interactions are an important contribution to the excimer state and to several of the higher states.

V. SUPPLEMENTARY MATERIAL

The data that supports the findings of this study are available within the article and its supplementary material. See the supplementary material for vertical excitations energies, oscillator strengths, omega matrices (with fragmentation scheme), orbital analysis, and S_0 and S_1 optimized geometries cartesian coordinates for tetracene monomer and dimer. For the latter, intermonomer CT values and DFT/MRCI reference active space tests are also included.

ACKNOWLEDGMENTS

This study was financed in part by the Coordenação de Aperfeiçoamento de Pessoal de Nível Superior - Brasil (CAPES) - Finance Code 001. The authors acknowledge the computer time provided by the School of Pharmaceutical Science and Technology (SPST) at Tianjin University, Tianjin, China, on the computer cluster Arran. The authors acknowledge the High Performance Computing Center (HPCC) at Texas Tech University for providing computational resources that have contributed to the research results reported within this paper. URL: http://www.hpcc.ttu.edu. MTC acknowledges the Conselho Nacional de Desenvolvimento Científico e Tecnológico (CNPq) and the Fundação de Apoio à Pesquisa do Estado

do Rio de Janeiro (FAPERJ), within the Bolsa Nota 10 program for financial support. MTC and MB thank the support of the FetOpen grant BoostCrop (Grant agreement 828753) and the project Equip@Meso (ANR-10-EQPX-29-01). TAN likes to thank the Laboratoire d'Excellence iMUST. This work was supported by the Center for Integrated Nanotechnologies (Project No. 2019BC0064), an Office of Science User Facility operated for the U.S. Department of Energy Office of Science by Los Alamos National Laboratory (Contract No. 89233218CNA000001) and Sandia National Laboratories (Contract No. DE-NA-0003525).

DATA AVAILABILITY

The data that supports the findings of this study are available within the article and its supplementary material.

REFERENCES

[1] O. Ostroverkhova, Chem. Rev. **116**, 13279 (2016).

[2] J.E. Anthony, Angew. Chemie Int. Ed. **47**, 452 (2008).

[3] Y.-W. Son, M.L. Cohen, and S.G. Louie, Nature **444**, 347 (2006).

[4] A. Candian and C.J. Mackie, Int. J. Quantum Chem. **117**, 146 (2017).

[5] M. Nakano and B. Champagne, J. Phys. Chem. Lett. **6**, 3236 (2015).

[6] D. Casanova, Chem. Rev. **118**, 7164 (2018).

[7] P.M. Zimmerman, F. Bell, D. Casanova, and M. Head-Gordon, J. Am. Chem. Soc. **133**, 19944 (2011).

[8] X. Feng, A. V. Luzanov, and A.I. Krylov, J. Phys. Chem. Lett. **4**, 3845 (2013).

[9] L.E. Aguilar Suarez, M.F.S.J. Menger, and S. Faraji, Mol. Phys. **8976**, 1 (2020).

[10] J. Han, D.R. Rehn, T. Buckup, and A. Dreuw, J. Phys. Chem. A (2020) DOI: 10.1021/acs.jpca.0c07236.

[11] C.B. Dover, J.K. Gallaher, L. Frazer, P.C. Tapping, A.J. Petty, M.J. Crossley, J.E. Anthony, T.W. Kee, and T.W. Schmidt, Nat. Chem. **10**, 305 (2018).

[12] M.T. Trinh, A. Pinkard, A.B. Pun, S.N. Sanders, E. Kumarasamy, M.Y. Sfeir, L.M. Campos, X. Roy, and X.-Y. Zhu, Sci. Adv. **3**, e1700241 (2017).

[13] T. Minami and M. Nakano, J. Phys. Chem. Lett. **3**, 145 (2012).

[14] F. Plasser, H. Pašalić, M.H. Gerzabek, F. Libisch, R. Reiter, J. Burgdörfer, T. Müller, R. Shepard, and H. Lischka, Angew. Chemie Int. Ed. **52**, 2581 (2013).

[15] E. Posenitskiy, M. Rapacioli, B. Lepetit, Di. Lemoine, and F. Spiegelman, Phys. Chem. Chem. Phys. **21**, 12139 (2019).

[16] F. Spillebout, D. Bégué, I. Baraille, and J.M. Shaw, Energy & Fuels **28**, 2933 (2014).

[17] M. Krämer, P.M. Dohmen, W. Xie, D. Holub, A.S. Christensen, and M. Elstner, J. Chem. Theory Comput. **16**, 4061 (2020).

[18] A. Kubas, F. Hoffmann, A. Heck, H. Oberhofer, M. Elstner, and J. Blumberger, J. Chem. Phys. **140**, 104105 (2014).

[19] P.B. Lutz and C.A. Bayse, Phys. Chem. Chem. Phys. **15**, 9397 (2013).

[20] E. Titov, A. Humeniuk, and R. Mitrić, Phys. Chem. Chem. Phys. **20**, 25995 (2018).

[21] B. Shi, D. Nachtigallová, A.J.A. Aquino, F.B.C. Machado, and H. Lischka, Phys. Chem. Chem. Phys. **21**, 9077 (2019).

[22] H. Yamagata, J. Norton, E. Hontz, Y. Olivier, D. Beljonne, J.L. Brédas, R.J. Silbey, and F.C. Spano, J. Chem. Phys. **134**, 204703 (2011).

[23] X. Feng and A.I. Krylov, Phys. Chem. Chem. Phys. **18**, 7751 (2016).

[24] J.A. Katul and A.B. Zahlan, J. Chem. Phys. **47**, 1012 (1967).

[25] M.A. Iannone and G.W. Scott, Chem. Phys. Lett. **171**, 569 (1990).

[26] C. Schouder, A.S. Chatterley, F. Calvo, L. Christiansen, and H. Stapelfeldt, Struct. Dyn. **6**, 044301 (2019).

[27] N.J. Silva, F.B.C. Machado, H. Lischka, and A.J.A. Aquino, Phys. Chem. Chem. Phys. **18**, 22300 (2016).

[28] P.M. Zimmerman, C.B. Musgrave, and M. Head-Gordon, Acc. Chem. Res. **46**, 1339 (2013).

[29] N. Elfers, I. Lyskov, J.D. Spiegel, and C.M. Marian, J. Phys. Chem. C **120**, 13901 (2016).

[30] G. Tao, J. Chem. Phys. **151**, 054308 (2019).

[31] S. Ito, T. Nagami, and M. Nakano, J. Photochem. Photobiol. C Photochem. Rev. **34**, 85 (2018).

[32] F. Plasser and H. Lischka, J. Chem. Theory Comput. **8**, 2777 (2012).

[33] F. Plasser, M. Wormit, and A. Dreuw, J. Chem. Phys. **141**, 024106 (2014).

[34] F. Plasser, "TheoDORE: A package for theoretical density, orbital relaxation, and exciton analysis", available from http://theodore-qc.sourceforge.net.

[35] J.B. Birks, Reports Prog. Phys. **38**, 903 (1975).

[36] Q. Ge and M. Head-Gordon, J. Chem. Theory Comput. **14**, 5156 (2018).

[37] T. Azumi, A.T. Armstrong, and S.P. McGlynn, J. Chem. Phys. **41**, 3839 (1964).

[38] T.M. Cardozo, A.P. Galliez, I. Borges, F. Plasser, A.J.A. Aquino, M. Barbatti, and H. Lischka, Phys. Chem. Chem. Phys. **21**, 13916 (2019).

[39] M. Elstner, D. Porezag, G. Jungnickel, J. Elsner, M. Haugk, T. Frauenheim, S. Suhai, and G. Seifert, Phys. Rev. B **58**, 7260 (1998).

[40] A. Humeniuk and R. Mitrić, J. Chem. Phys. **143**, 134120 (2015).

[41] J.J. Kranz, M. Elstner, B. Aradi, T. Frauenheim, V. Lutsker, A.D. Garcia, and T.A. Niehaus, J. Chem. Theory Comput. **13**, 1737 (2017).

[42] J. Hoche, H.-C. Schmitt, A. Humeniuk, I. Fischer, R. Mitrić, and M.I.S. Röhr, Phys. Chem. Chem.

Phys. **19**, 25002 (2017).

[43] Y. Jung, R.C. Lochan, A.D. Dutoi, and M. Head-Gordon, J. Chem. Phys. **121**, 9793 (2004).

[44] J.-D. Chai and M. Head-Gordon, Phys. Chem. Chem. Phys. **10**, 6615 (2008).

[45] A. Hellweg, S.A. Grün, and C. Hättig, Phys. Chem. Chem. Phys. **10**, 4119 (2008).

[46] M. Gaus, Q. Cui, and M. Elstner, J. Chem. Theory Comput. **7**, 931 (2011).

[47] T. Yanai, D.P. Tew, and N.C. Handy, Chem. Phys. Lett. **393**, 51 (2004).

[48] A. Dreuw and M. Wormit, Wiley Interdiscip. Rev. Comput. Mol. Sci. **5**, 82 (2015).

[49] J. Schirmer, Phys. Rev. A **26**, 2395 (1982).

[50] S. Grimme and M. Waletzke, J. Chem. Phys. **111**, 5645 (1999).

[51] C.M. Marian, A. Heil, and M. Kleinschmidt, WIREs Comput. Mol. Sci. **9**, e1394 (2019).

[52] B. Shi, D. Nachtigallová, A.J.A. Aquino, F.B.C. Machado, and H. Lischka, J. Chem. Phys. **150**, 124302 (2019).

[53] B. Shi, D. Nachtigallová, A.J.A. Aquino, F.B.C. Machado, and H. Lischka, J. Phys. Chem. Lett. **10**, 5592 (2019).

[54] S.A. Bäppler, F. Plasser, M. Wormit, and A. Dreuw, Phys. Rev. A - At. Mol. Opt. Phys. **90**, 45 (2014).

[55] F. Furche, R. Ahlrichs, C. Hättig, W. Klopper, M. Sierka, and F. Weigend, Wiley Interdiscip. Rev. Comput. Mol. Sci. **4**, 91 (2014).

[56]TURBOMOLE V7.2 2017, a development of University of Karlsruhe and Forschungszentrum Karlsruhe GmbH, 1989-2007,TURBOMOLE GmbH, since 2007; available from http://www.turbomole.com.

[57] C. Hättig and F. Weigend, J. Chem. Phys. **113**, 5154 (2000).

[58] C. Hättig, J. Chem. Phys. **118**, 7751 (2003).

[59] A. Köhn and C. Hättig, J. Chem. Phys. **119**, 5021 (2003).

[60] F. Weigend, M. Häser, H. Patzelt, and R. Ahlrichs, Chem. Phys. Lett. **294**, 143 (1998).

[61] F. Neese, WIREs Comput. Mol. Sci. **2**, 73 (2012).

[62] F. Neese, WIREs Comput. Mol. Sci. **8**, 4 (2018).

[63] M. J. Frisch, G. W. Trucks, H. B. Schlegel, G. E. Scuseria, M. A. Robb, J. R. Cheeseman, G. Scalmani, V. Barone, B. Mennucci, G. A. Petersson, H. Nakatsuji, M. Caricato, X. Li, H. P. Hratchian, A. F. Izmaylov, J. Bloino, G. Zheng, J. L. Sonnenberg, M. Hada, M. Ehara, K. Toyota, R. Fukuda, J. Hasegawa, M. Ishida, T. Nakajima, Y. Honda, O. Kitao, H. Nakai, T. Vreven, J. A. Montgomery, Jr., J. E. Peralta, F. Ogliaro, M. Bearpark, J. J. Heyd, E. Brothers, K. N. Kudin, V. N. Staroverov, T. Keith, R. Kobayashi, J. Normand, K. Raghavachari, A. Rendell, J. C. Burant, S. S. Iyengar, J. Tomasi, M. Cossi, N. Rega, J. M. Millam, M. Klene, J. E. Knox, J. B. Cross, V. Bakken, C. Adamo, J. Jaramillo, R. Gomperts, R. E. Stratmann, O. Yazyev, A. J. Austin, R. Cammi, C. Pomelli, J. W. Ochterski, R. L. Martin, K. Morokuma, V. G. Zakrzewski, G. A. Voth, P. Salvador, J. J. Dannenberg, S. Dapprich, A. D. Daniels, O. Farkas, J. B. Foresman, J. V. Ortiz, J. Cioslowski, and D. J. Fox, Gaussian 09, Revision E.01, Gaussian, Inc., Wallingford CT, 2013.

[64] F. Weigend, Phys. Chem. Chem. Phys. **8**, 1057 (2006).

[65] A. Hellweg, C. Hättig, S. Höfener, and W. Klopper, Theor. Chem. Acc. **117**, 587 (2007).

[66] S. Grimme, S. Ehrlich, and L. Goerigk, J. Comput. Chem. **32**, 1456 (2011).

[67] S. Grimme, J. Antony, S. Ehrlich, and H. Krieg, J. Chem. Phys. **132**, 154104 (2010).

[68] I. Lyskov, M. Kleinschmidt, and C.M. Marian, J. Chem. Phys. **144**, 034104 (2016).

[69] A. Heil, M. Kleinschmidt, and C.M. Marian, J. Chem. Phys. **149**, 164106 (2018).

[70] M. Kleinschmidt, C.M. Marian, M. Waletzke, and S. Grimme, J. Chem. Phys. **130**, 044708 (2009).

[71] A.D. Becke, J. Chem. Phys. **98**, 1372 (1993).

[72] R. Crespo-Otero and M. Barbatti, J. Chem. Phys. **134**, 164305 (2011).

[73] F. Weigend and R. Ahlrichs, Phys. Chem. Chem. Phys. **7**, 3297 (2005).

[74] B. Hourahine, B. Aradi, V. Blum, F. Bonafé, A. Buccheri, C. Camacho, C. Cevallos, M.Y. Deshaye, T. Dumitrică, A. Dominguez, S. Ehlert, M. Elstner, T. van der Heide, J. Hermann, S. Irle, J.J. Kranz, C. Köhler, T. Kowalczyk, T. Kubař, I.S. Lee, V. Lutsker, R.J. Maurer, S.K. Min, I. Mitchell, C. Negre, T.A. Niehaus, A.M.N. Niklasson, A.J. Page, A. Pecchia, G. Penazzi, M.P. Persson, J. Řezáč, C.G. Sánchez, M. Sternberg, M. Stöhr, F. Stuckenberg, A. Tkatchenko, V.W.Z. Yu, and T. Frauenheim, J. Chem. Phys. **152**, 124101 (2020).

[75] V.Q. Vuong, J. Akkarapattiakal Kuriappan, M. Kubillus, J.J. Kranz, T. Mast, T.A. Niehaus, S. Irle, and M. Elstner, J. Chem. Theory Comput. **14**, 115 (2018).

[76] M. Gaus, A. Goez, and M. Elstner, J. Chem. Theory Comput. **9**, 338 (2013).

[77] L. Zhechkov, T. Heine, S. Patchkovskii, G. Seifert, and H.A. Duarte, J. Chem. Theory Comput. **1**, 841 (2005).

[78] A.K. Rappe, C.J. Casewit, K.S. Colwell, W.A. Goddard, and W.M. Skiff, J. Am. Chem. Soc. **114**, 10024 (1992).

[79] Jmol: an open-source Java viewer for chemical structures in 3D. http://www.jmol.org/.

[80] R. Nieman, A.J.A. Aquino, and H. Lischka, J. Chem. Phys. **152**, 044306 (2020).

[81] H. Takeuchi, Comput. Theor. Chem. **1021**, 84 (2013).

[82] C. Gonzalez and E.C. Lim, J. Phys. Chem. A **104**, 2953 (2000).

[83] S.M. Ryno, C. Risko, and J.-L. Brédas, Chem. Mater. **28**, 3990 (2016).

[84] S. Tsuzuki, K. Honda, T. Uchimaru, and M. Mikami, J. Chem. Phys. **120**, 647 (2004).

[85] C.M. Marian and N. Gilka, J. Chem. Theory Comput. **4**, 1501 (2008).

[86] F. Bettanin, L.F.A. Ferrão, M. Pinheiro, A.J.A. Aquino, H. Lischka, F.B.C. Machado, and D. Nachtigallova, J. Chem. Theory Comput. **13**, 4297 (2017).

[87] D. Biermann and W. Schmidt, J. Am. Chem. Soc. **102**, 3163 (1980).

[88] N. Nijegorodov, V. Ramachandran, and D.P. Winkoun, Spectrochim. Acta Part A Mol. Biomol.

Spectrosc. **53**, 1813 (1997).

[89] P. Elliott, S. Goldson, C. Canahui, and N.T. Maitra, Chem. Phys. **391**, 110 (2011).

[90] P.M. Zimmerman, Z. Zhang, and C.B. Musgrave, Nat. Chem. **2**, 648 (2010).

[91] G.D. Scholes and G. Rumbles, Nat. Mater. **5**, 683 (2006).